Dynamical and Microphysical Retrieval from Doppler Radar Observations Using a Cloud Model and Its Adjoint. Part I: Model Development and Simulated Data Experiments

JUANZHEN SUN AND N. ANDREW CROOK

National Center for Atmospheric Research, Boulder, Colorado*

(Manuscript received 12 April 1996, in final form 12 December 1996)

ABSTRACT

The purpose of the research reported in this paper is to develop a variational data analysis system that can be used to assimilate data from one or more Doppler radars. In the first part of this two-part study, the technique used in this analysis system is described and tested using data from a simulated warm rain convective storm. The analysis system applies the 4D variational data assimilation technique to a cloud-scale model with a warm rain parameterization scheme. The 3D wind, thermodynamical, and microphysical fields are determined by minimizing a cost function, defined by the difference between both radar observed radial velocities and reflectivities (or rainwater mixing ratio) and their model predictions. The adjoint of the numerical model is used to provide the sensitivity of the cost function with respect to the control variables.

Experiments using data from a simulated convective storm demonstrated that the variational analysis system is able to retrieve the detailed structure of wind, thermodynamics, and microphysics using either dual-Doppler or single-Doppler information. However, less accurate velocity fields are obtained when single-Doppler data were used. In both cases, retrieving the temperature field is more difficult than the retrieval of the other fields. Results also show that assimilating the rainwater mixing ratio obtained from the reflectivity data results in a better performance of the retrieval procedure than directly assimilating the reflectivity. It is also found that the system is robust to variations in the Z–q_r relation, but the microphysical retrieval is quite sensitive to parameters in the warm rain scheme. The technique is robust to random errors in radial velocity and calibration errors in reflectivity.

1. Introduction

During the past few decades, observations from Doppler radars have been widely used in diagnostic studies of convective systems, severe weather detection, and short-term forecasting. With the deployment of the NEXRAD network in the 1990s, there has been an increased interest in the possibility of operational cloud-scale numerical forecasting. One of the major challenges in cloud-scale numerical weather prediction is obtaining accurate initial conditions. Doppler radars, which provide observations of radial velocity and reflectivity with a spatial resolution of a few hundred meters every 3–10 min, are practically the only instrument capable of sampling the four-dimensional structure of storm-scale flows. To specify the state of the atmosphere using these data, it is necessary to develop techniques to derive detailed meteorological fields that are not directly measured by Doppler radars. The quantitative information obtained thereby will not only provide initial conditions for cloud-scale numerical models but also help improve operational forecasting skills and enhance our understanding of precipitating weather systems.

Over the past few decades, various methods have been developed to infer detailed information from single or multiple-Doppler observations. Using observations from a single-Doppler radar, it has been shown that the boundary layer flow can be retrieved with reasonable accuracy (e.g., Tuttle and Foote 1990; Qiu and Xu 1992; Laroche and Zawadzki 1994; Shapiro et al. 1995). With the availability of multiple-Doppler radars, researchers have demonstrated that the three-dimensional wind field can be derived through the use of the mass continuity equation (Armijo 1969) and the thermodynamic fields can then be obtained with the aid of the equations of motion (Gal-Chen 1978; Hane and Scott 1978; Hane et al. 1981; Roux et al. 1985).

Methods to diagnose microphysical variables from radar data have also been examined by a number of researchers. Rutledge and Hobbs (1983, 1984), followed by Ziegler (1985, 1988), employed detailed diagnostic kinematical cloud models to derive the thermodynamic

*The National Center for Atmospheric Research is sponsored by the National Science Foundation.

Corresponding author address: Dr. Juanzhen Sun, NCAR/MMM Division, P.O. Box 3000, Boulder, CO 80307-3000.
E-mail: sunj@ncar.ucar.edu

and microphysical fields using dual-Doppler synthesized wind fields. Hauser and Amayenc (1986) used the continuity equation for total water content to diagnose the microphysical variables, assuming wind and thermodynamic fields were given through a dynamic retrieval method (Roux et al. 1985). All of the abovementioned studies in microphysical retrieval used the assumption that the cloud system was in steady state. Verlinde and Cotton (1990) examined the performance of the microphysical retrieval using an algorithm of the Rutledge–Ziegler type in a situation where the steady-state assumption was clearly violated. They found that the microphysical and thermodynamic fields were either overestimated or underestimated, indicating that a knowledge of the time history of the microphysical data was important in the developing and dissipating stages of storms.

In recent years, considerable effort has been devoted to the field of four-dimensional variational (4DVAR) data assimilation through the use of adjoint models. The adjoint formalism was first proposed by Le Dimet (1982) for meteorological applications and was then implemented by Derber (1985), Lewis and Derber (1985), Courtier (1985), Le Dimet and Talagrand (1986), Talagrand and Courtier (1987), Navon et al. (1992), Zupanski (1993), and Zou et al. (1993a,b), among others. Most of these applications have been for the initialization of large-scale numerical models. The problem of 4DVAR for the convective scale is different in that it aims more at the generation of unobserved fields, rather than at optimal filtering as for the large scale. Sun et al. (1991) developed the adjoint dynamic retrieval technique and demonstrated that the three-dimensional wind and thermodynamic fields could be obtained from observations of a single-Doppler radar. Applications of this technique to a gust front case from the Phoenix II experiment showed encouraging results (Sun and Crook 1994). Using a kinematic microphysical model, Verlinde and Cotton (1993) demonstrated that, given the dynamical variables, the microphysical variables could be retrieved using the adjoint technique. The promising results obtained in these studies has led us to develop a variational Doppler radar analysis system (VDRAS) that is aimed at retrieving the three-dimensional wind, temperature, pressure, and microphysical fields in moist convective flows from single- or multiple-Doppler radar observations. By fitting a three-dimensional, time-dependent cloud resolving model to a time series of observations using a 4DVAR data assimilation technique, the atmospheric state containing dynamically consistent information of wind, thermodynamics, and microphysics can be determined.

A cloud model contains parameterized moist processes that are often characterized by on/off switches. These processes are often highly nonlinear and discontinuous. Since the adjoint model was initially derived for differentiable systems of equations, a model with discontinuous moist processes may present some problems. Recently, as more and more researchers have begun to include physical parameterization processes in their 4DVAR systems, the problems related to on/off switches have drawn attention in the data assimilation community (Douady and Talagrand 1990; Vukicevic and Errico 1993; Zou et al. 1993b; Zupanski and Mesinger 1995; Verlinde and Cotton 1993; Bao and Kuo 1995, Bao and Warner 1993; Xu 1996a,b; Zou 1995). Theoretical studies by Bao and Kuo (1995) and Xu (1996a,b) suggested that a mathematically rigorous adjoint of the physical parameterization scheme involving on/off switches must consider the variation of the switching time (the physical time into the run at which the parameterization scheme switches on or off) with respect to the perturbation of the control variables. Nevertheless, experimental studies by Zou et al. (1993b), Zou (1995), Verlinde and Cotton (1993), and Zupanski and Mesinger (1995) showed that their minimization processes were well behaved while keeping the on/off switches the same as in the basic state. However, in the latter two studies, smoothing by fitting a function of time was applied to eliminate some of the switches.

The main purpose of this paper is to describe the new variational Doppler radar analysis system and demonstrate its ability in retrieving the 3D wind, thermodynamical, and microphysical structure of convective storms. Issues associated with the adjoint of moist processes will also be discussed. We test the retrieval technique on simulated data of moist convection initiated from a warm, moist bubble. In Part II of this paper, the retrieval technique will be tested on airmass storms observed during the Convection and Precipitation/Electrification Experiment. This paper is organized as follows. Section 2 describes the numerical model and the physical parameterization schemes. The variational data assimilation technique used in VDRAS will be described in section 3. Some special treatments of the moist processes in the adjoint model will also be addressed in this section. In section 4, the control simulation is described and the results of retrieval experiments are presented. In section 5, summary and discussion are given.

2. Numerical model

a. Basic equations

The model contains six prognostic equations. They are the three momentum equations, the thermodynamic equation, the rainwater equation, and the total water equation. Using the anelastic approximation, the momentum equations are written as

$$\frac{d\bar{\rho}u}{dt} = -\frac{\partial p'}{\partial x} + \nu\nabla^2\bar{\rho}u, \tag{2.1}$$

$$\frac{d\bar{\rho}v}{dt} = -\frac{\partial p'}{\partial y} + \nu\nabla^2\bar{\rho}v, \tag{2.2}$$

$$\frac{d\bar{\rho}w}{dt} = -\frac{\partial p'}{\partial z} + g\bar{\rho}\left(\frac{T'}{T} + 0.61q_v' - q_c - q_r\right) + \nu\nabla^2\bar{\rho}w. \quad (2.3)$$

The mass continuity equation is written as

$$\frac{\partial\bar{\rho}u}{dx} + \frac{\partial\bar{\rho}v}{dy} + \frac{\partial\bar{\rho}w}{dz} = 0. \quad (2.4)$$

Here, u, v, and w are the wind velocities and q_v, q_c, and q_r are mixing ratios for water vapor, cloud water, and rain water, respectively; T, ρ, and p are the temperature, the density of air, and the pressure, respectively. The primed variables represent the deviations from the initial unperturbed state whose variables are denoted with overbars. The quantity ν is the eddy viscosity. The perturbation pressure p' is a diagnostic variable that can be obtained by solving the Poisson equation

$$\nabla^2 p' = -\nabla\cdot(\boldsymbol{v}\cdot\nabla\bar{\rho}\boldsymbol{v}) + g\bar{\rho}\frac{\partial}{\partial z}\left(\frac{T'}{T} + 0.61q_v' - q_c - q_r\right). \quad (2.5)$$

The thermodynamic equation is written in terms of liquid water potential temperature, θ_l, following Tripoli and Cotton (1981):

$$\frac{d\bar{\rho}\theta_l}{dt} = -\frac{L_v\bar{\rho}}{c_pT}\frac{\theta_l^2}{\theta}\frac{dV_{\mathrm{Tm}}q_r}{dz} + \kappa\nabla^2\bar{\rho}\theta_l. \quad (2.6)$$

The variable V_{Tm} is the mass-weighted terminal velocity, which will be described later. The quantity κ is the diffusivity of liquid water potential temperature and L_v is the latent heat of vaporization. The liquid water potential temperature is a conserved quantity with respect to condensation and evaporation. It is defined by

$$\theta_l = \theta\left(1 - \frac{L_v}{c_pT}(q_c + q_r)\right). \quad (2.7)$$

The equations governing the rainwater q_r and total water content q_t are

$$\frac{d\bar{\rho}q_r}{dt} = R_c + R_a + R_e + \bar{\rho}\frac{dV_{\mathrm{Tm}}q_r}{dz} + \kappa\nabla^2\bar{\rho}q_r, \quad (2.8)$$

$$\frac{d\bar{\rho}q_t}{dt} = \bar{\rho}\frac{dV_{\mathrm{Tm}}q_r}{dz} + \kappa\nabla^2\bar{\rho}q_t. \quad (2.9)$$

Here, R_a is the transfer rate from cloud water to rainwater due to autoconversion, R_c is the transfer rate from cloud water to rainwater due to accretion, and R_e is the evaporation rate resulting from the evaporation of raindrops in subsaturated air. The parameterization of these three quantities will be given later. The total water content q_t is defined by

$$q_t = \begin{cases} q_c + q_{\mathrm{vs}} + q_r, & \text{if } (q_v \geq q_{\mathrm{vs}}) \\ q_v + q_r, & \text{if } (q_v < q_{\mathrm{vs}}). \end{cases} \quad (2.10)$$

The temperature and cloud water mixing ratios are diagnosed from the prognostic variables by assuming that all vapor in excess of the saturation value is converted to cloud water. These variables are related through

$$T = \left(\frac{p}{p_0}\right)^{R/c_p}\theta_l\left(1 + \frac{l_v}{c_pT}(q_c + q_r)\right), \quad (2.11)$$

and

$$q_c = \begin{cases} (q_t - q_{\mathrm{vs}} - q_r), & \text{if } (q_v \geq q_{\mathrm{vs}}) \\ 0, & \text{if } (q_v < q_{\mathrm{vs}}), \end{cases} \quad (2.12)$$

where q_{vs} is the saturation mixing ratio given by

$$q_{\mathrm{vs}} = \frac{3.8}{p}\exp\left(17.27\frac{T - 273.16}{T - 35.86}\right). \quad (2.13)$$

A bisection iteration scheme is used to obtain the temperature from Eqs. (2.11), (2.12), and (2.13). The temperature is computed within 0.01°C accuracy, which generally takes less than 10 iterations.

In this model, the liquid water potential temperature is chosen as the thermodynamical variable so that only two prognostic equations are required for the microphysics (q_r and q_t). As will be seen in the following section, the number of control variables of the optimization problem depends on the number of prognostic variables in the model. A model system with two microphysical prognostic equations will obviously reduce the number of control variables compared to a model system that requires three microphysical prognostic equations (e.g., q_c, q_r, and q_v).

All the model variables are scaled by their typical values and the numerical model is coded in terms of dimensionless variables. The reason for doing this is to balance the magnitude of the different variables such that each variable has a similar weight during the optimization, and hence a better convergence rate (e.g., Gill et al. 1981).

b. Physical processes

The physical processes allowed in this model are condensation and evaporation of cloud water (implicit in θ_l), evaporation of raindrops in subsaturated air, autoconversion of cloud to rain, accretion of cloud by rain, and sedimentation of rain.

Autoconversion and evaporation of rain are parameterized following Kessler (1969) as

$$R_a = \begin{cases} \alpha(q_c - q_{\mathrm{crit}}), & \text{for } q_c > q_{\mathrm{crit}} \\ 0, & \text{for } q_c < q_{\mathrm{crit}}, \end{cases} \quad (2.14)$$

$$R_e = \beta(q_v - q_{\mathrm{vs}})(\rho q_r)^{0.65}, \quad (2.15)$$

and we are presently setting $\alpha = 0.001\ \mathrm{s}^{-1}$, $q_{\mathrm{crit}} = 1.5\ \mathrm{g\ kg}^{-1}$, and $\beta = 0.0486\ \mathrm{s}^{-1}$. The mass-weighted velocity of rainwater, required to calculate sedimentation, is calculated assuming a Marshall–Palmer drop-size distribution. It is given by

$$V_{\mathrm{Tm}} = 5.40a(\rho q_r)^{0.125}. \quad (2.16)$$

The quantity a is a correction factor defined by $a = (p_0/\bar{p})^{0.4}$, where $\bar{p}$ is the base-state pressure and p_0 is the pressure at the ground. The rainwater mixing ratio q_r is in units g kg^{-1}. Accretion is parameterized using the expression

$$R_c = \gamma q_c\, q_r^{7/8}, \quad (2.17)$$

where γ is set to 0.002 s^{-1}, following Miller and Pearce (1974).

3. Description of the technique used in VDRAS

a. Definition of the cost function

The four-dimensional variational data assimilation technique is applied in this analysis system. The objective is to find an initial state that can, upon model integration, produce output parameters matching the observations as closely as possible. A cost function measuring the misfit between the model and data is defined in terms of the radar observed variables, that is, the radial velocity and reflectivity. Assuming that the observational errors of each field are uncorrelated in space and time, the cost function J_1 is given by

$$J_1 = \sum_{\sigma,\tau,i} [\eta_v(V_{r,i} - V_{r,i}^{\mathrm{ob}})^2 + \eta_z(Z - Z_i^{\mathrm{ob}})^2] + J_b + J_p. \quad (3.1)$$

where σ represents the spatial domain and τ represents the temporal domain. The index i stands for the ith radar. The quantities $V_{r,i}^{\mathrm{ob}}$ and Z_i^{ob} are observations of the radial velocity and reflectivity, respectively, from the ith radar. Here, $V_{r,i}$ and Z are their model counterparts. These two quantities are not direct model outputs but are calculated using the model outputs of Cartesian velocity and rainwater mixing ratio q_r. The relation between Z and q_r is derived analytically by assuming the Marshal–Palmer distribution of raindrop size. Assuming $n_0 = 8 \times 10^6$ mm^{-4}, the result is

$$Z = 2.04 \times 10^4(\rho q_r)^{1.75}, \quad (3.2)$$

where Z is the reflectivity (units of mm^6 m^{-3}). If the reflectivity is in units of dBZ, the Z–q_r relation becomes

$$Z = 43.1 + 17.5 \log(\rho q_r). \quad (3.3)$$

From Eq. (3.2) or (3.3), a model-predicted reflectivity can be calculated using the model output q_r. On the other hand, a set of rainwater data q_r^{ob} can be obtained from the reflectivity observations. If we take q_r^{ob} as observations, another cost function J_2 can be defined as

$$J_2 = \sum_{\sigma,\tau,i} [\eta_v(V_{r,i} - V_{r,i}^{\mathrm{ob}})^2 + \eta_q(q_r - q_{r,i}^{\mathrm{ob}})^2] + J_b + J_p, \quad (3.4)$$

where q_r is the model-predicted rainwater mixing ratio (units of g kg^{-1}). The radial velocity $V_{r,i}$ in both Eqs. (3.1) and (3.4) is calculated using the Cartesian velocity components (u, v, w) from the model integration through the relation

$$V_{r,i} = u\frac{x - x_i}{r_i} + v\frac{y - y_i}{r_i} + (w - V_{\mathrm{Tm}})\frac{z - z_i}{r_i}, \quad (3.5)$$

where V_{Tm} is the terminal velocity of the precipitation given by Eq. (2.16). Here, r_i is the distance between a grid point (x, y, z) and the ith radar location (x_i, y_i, z_i).

Either J_1 or J_2 can be used as the cost function in a retrieval experiment. Most experiments presented in section 4 of this paper used the cost function J_2. Experiments using J_1 as the cost function will also be discussed and compared with those using J_2.

The quantities η_v, η_z, and η_q in Eqs. (3.1) and (3.4) are weighting coefficients for radial velocity, reflectivity, and rainwater mixing ratio, respectively. In the current study with simulated data, these weighting coefficients are simply taken as constants. The value of ρ_z or ρ_q relative to ρ_v is determined such that the two terms in the cost function have similar magnitude. It should be noted that, in both Eqs. (3.1) and (3.4), we have assumed that the observational errors are uncorrelated and these errors are evenly distributed in space and time. In reality, however, this is usually not the case. In Part II of this study, we will discuss methods to estimate the error covariance matrix when real data are employed.

In Eq. (3.1) and (3.4), Z_i^{ob} and $q_{r,i}^{\mathrm{ob}}$ denote the observations of the reflectivity and rainwater mixing ratio from the ith radar. It is important to note that, although ideally different radars should give the same observations of reflectivity, in reality the reflectivity observed and hence the rainwater estimated by different radars can have some differences due to instrumentation or calibration error, attenuation, and beam blockage.

The parameters J_b and J_p in the cost functions J_1 and J_2 represent background and penalty terms, respectively. Since radar data are concentrated only in the region where scatterers exist, there are no radar observations outside that region. The flow field in the data-void region is constrained toward the background provided by some other sources of observations by adding a background term J_b to the cost function. The general form of the background term can be written as

$$J_b = (\mathbf{x} - \mathbf{x}_b)^{\mathrm{T}}\, \mathbf{B}^{-1}\, (\mathbf{x} - \mathbf{x}_b), \quad (3.6)$$

where $\mathbf{x}$ represents model variables in vector form and $\mathbf{x}_b$ stands for the background information. Here, $\mathbf{B}$ is the covariance matrix of the background error. More discussion on the background term will be given in section 4. The quantity J_p in the cost function represents the spatial and temporal smoothness penalty functions. The formulation and effect of these functions were discussed in Sun and Crook (1994).

A constrained variational problem is constructed by using either one of the two cost functions J_1 and J_2 with the model equations given in section 2 representing the constraints. The initial conditions (IC) of the numerical

model are the control variables, assuming the boundary conditions and the model parameters are given. Therefore, the variational problem can be stated thus: find a set of IC of the numerical model that minimizes the cost function J_1 or J_2. This problem can be solved by redefining it so that it becomes a problem of unconstrained minimization. Standard procedures on minimization for problems of this type can be found in textbooks on optimization (e.g., Gill et al. 1981; Luenberger 1984). The minimization algorithm used in this study is Nocedal's limited memory, quasi-Newton conjugate gradient method (Liu and Nocedal 1989). The objective in the minimization method is to find a search direction, d^k, and a step length, α^k, at the kth iteration that will lead to a new IC and reduce the cost function, namely, $J(x_0^k + \alpha^k d^k) \leq J(x_0^k)$. The search direction d^k is calculated using the information of the cost function and its gradient. The cost function can be computed by integrating the model forward and the gradient is obtained by integrating the adjoint model (described in the appendix) backward in time.

b. *Special treatment of the moist processes in the adjoint model*

The cloud model described in the last section contains a number of physical parameterization processes. These moist processes have two general characteristics: one is that they are associated with on/off switches; the other is that the parameterization schemes are often highly nonlinear. Since the adjoint model was originally derived for a differentiable system of equations and used to provide first-order derivative information of the cost function, moist processes with nondifferentiable on/off switches and a high degree of nonlinearity can cause difficulties in the minimization procedure. The first adjoint models with full physics were developed by keeping the on/off switches the same as in the basic state or, in other words, by ignoring the variation of the switching time caused by the perturbation in IC (Zou et al. 1993b; Vukicevic and Errico 1993; Zupanski and Mesinger 1995). Test results by Zou et al. (1993b) showed that the minimization procedure converged at a similar rate as the one with the adiabatic version of their model. Zupanski and Mesinger (1995) demonstrated that errors caused by discontinuous on/off switches were reduced by applying a selective vertical smoothing to the layers of transition in the Betts–Miller cumulus convective scheme. Using simple differential equations, Bao and Kuo (1995), Xu (1996a,b), and Zou (1995) gave rigorous mathematical derivations for physical processes that contain on/off switches. Their derivations all showed that additional terms appeared in the adjoint model if the change in the switching time due to an initial perturbation was considered. However, Zou (1995) also argued that, for a discretized numerical model, the switching time occurs at the same time step for both perturbed and basic-state solutions in regard to very small perturbations in the IC. ''Very small'' perturbations mean small enough to be able to ignore the higher-order terms and large enough to avoid machine round-off error. It should be noted that, in 4DVAR, the adjoint model is used for calculating the gradient of the cost function with respect to the IC and this gradient is derived for an infinitesimal perturbation. Zou (1995) showed that the additional terms due to differentiation of switches indicated by Xu (1996) do not seem to exist or are very small for a discretized model in her rainfall assimilation study.

In our study, the derivation of the adjoint of physical processes with on/off switches follows that of Zou (1993b); that is, the switching times are kept the same as in the forward integration of the prediction model. The adjoint model derived in this manner did not seem to cause any problem in the minimization. We have found, however, that the high degree of nonlinearity associated with the parameterization of some of the physical processes can cause serious problems for the minimization. Without any modification of the original parameterization schemes, we have found two schemes that can cause the minimization process to fail. One is the evaporation of rain given by Eq. (2.15); the other is the rainwater fall velocity given by Eq. (2.16). When the rainwater mixing ratio is close to zero, both parameterization schemes yield a very large gradient with respect to the rainwater mixing ratio. This can be easily shown by taking the derivative of Eqs. (2.15) and (2.16) with respect to q_r to yield

$$\frac{\partial R_e}{\partial q_r} = 0.65\beta\rho(q_v - q_{vs})(\rho q_r)^{-0.35}, \tag{3.7}$$

and

$$\frac{\partial V_{\mathrm{Tm}}}{\partial q_r} = 0.125 \times 5.40a(\rho q_r)^{-0.875}. \tag{3.8}$$

The large gradient associated with very small values of rainwater mixing ratio can cause an imbalance of the gradient among different control variables. The minimization fails to converge due to this type of ill-conditioning. To avoid this problem, the two schemes were slightly modified. First, the evaporation rate is kept constant for rainwater mixing ratios less than a critical value $q_{e\mathrm{crit}}$. Second, the rainwater fall velocity is modified such that the velocity is a constant for rainwater mixing ratios smaller than 0.05 g kg^{-1}. The scheme for evaporation of rain now becomes

$$R_e = \begin{cases} \beta(q_v - q_{vs})(\rho q_r)^{0.65}, & \text{if } q_r > q_{e\mathrm{crit}} \text{ g kg}^{-1} \\ \beta(q_v - q_{vs})(\rho q_{e\mathrm{crit}})^{0.65}, & \text{if } q_r \leq q_{e\mathrm{crit}} \text{ g kg}^{-1} \end{cases} \tag{3.9}$$

and the rainwater fall velocity is changed to

$$V_{\mathrm{Tm}} = \begin{cases} 5.40a(\rho q_r)^{0.125}, & \text{if } q_r > 0.05 \text{ g kg}^{-1} \\ 5.40a(0.05\rho)^{0.125}, & \text{if } 0 < q_r \le 0.05 \text{ g kg}^{-1}. \end{cases} \tag{3.10}$$

The derivatives in (3.12) and (3.13) now become

$$\frac{\partial R_e}{\partial q_r} = \begin{cases} 0.65(q_v - q_{vs})(\rho q_r)^{-0.35}, \\ \quad \text{if } q_r > q_{\mathrm{ecrit}} \text{ g kg}^{-1} \\ 0, \\ \quad \text{if } q_r \le q_{\mathrm{ecrit}} \text{ g kg}^{-1} \end{cases} \tag{3.11}$$

and

$$\frac{\partial V_{\mathrm{Tm}}}{\partial q_r} = \begin{cases} 0.125 \times 5.40a(\rho q_r)^{-0.875}, \\ \quad \text{if } q_r > 0.05 \text{ g kg}^{-1} \\ 0, \\ \quad \text{if } 0 < q_r \le 0.05 \text{ g kg}^{-1}. \end{cases} \tag{3.12}$$

In this way, the large gradient associated with very small rainwater mixing ratio is replaced by zero. The value of q_{ecrit} in Eqs. (3.9) and (3.11) will be given later in this section.

It should be noted that, in the governing equations, the velocity of rainwater is always multiplied by the rainwater mixing ratio to produce the precipitation rate, that is, $(dV_{\mathrm{Tm}}q_r)/(dz)$. As a result, the nonlinearity is greatly reduced since $(dV_{\mathrm{Tm}}q_r)/(dz) \propto q_r^{1.125}$. Other than in the precipitation term, V_{Tm} also appears in the cost functions (3.1) and (3.4) through the model-predicted radial velocity $V_{r,i}$, where its high nonlinearity will cause some problems.

The modifications described above make a great difference in the gradient calculation through the adjoint model but affect the forward model integration negligibly. In the following section, we will not apply these modifications to the control simulation through which the data are generated. They will only be used in the forward model integration and the backward adjoint integration in the assimilation runs.

As shown in the appendix, the adjoint model is the transpose of the tangent linear model and is used to provide first-order derivative information of the cost function. Therefore, how well the tangent linear model (TLM) solution approximates the nonlinear model solution determines how valid the gradient of the cost function is. Following Zou (1995), to verify the correctness of the TLM, one can define a function $\Phi(\alpha)$, given by

$$\Phi(\alpha) = \frac{F_n(x_0 + \alpha h) - F_n(x_0)}{\alpha G_n h}, \tag{3.13}$$

where F and G are the nonlinear model and the tangent linear model operators, respectively, as defined in the appendix. The quantity h is a normalized random vector and α is a scalar. Here $\Phi(\alpha)$ can be computed for a particular point or for all the points in the domain. In the latter case, the rms error for both the nonlinear model and the tangent linear model was compared. If the TLM approximates the nonlinear model well, one should expect to obtain a value of $\Phi(\alpha)$ close to unity for small values of α at any particular point. In order to examine how well the tangent linear solution approximates the nonlinear solution and how the special treatment described above affects the tangent linear approximation, three tests were performed to evaluate $\Phi(\alpha)$. Since the tests were performed on a CRAY-YMP supercomputer, which has 64-bit accuracy, we used 10^{-12} as the smallest value for α. In test 1, the original parameterization schemes were used. In test 2, the evaporation of rain follows Eq. (3.14) with q_{ecrit} set to 0.001 g kg^{-1}. The last test was similar to the second but the threshold q_{ecrit} was changed from 0.001 g kg^{-1} to 0.1 g kg^{-1}. Both the TLM and nonlinear model integrations started at t = 41.7 min and the length of the integration was 8.3 min, or 50 time steps. The results of these three tests are compared in Fig. 1 by plotting the change of $\Phi(\alpha)$ with α for (a) vertical velocity and (b) for rainwater mixing ratio. Here we show $\Phi(\alpha)$ summed over all points in

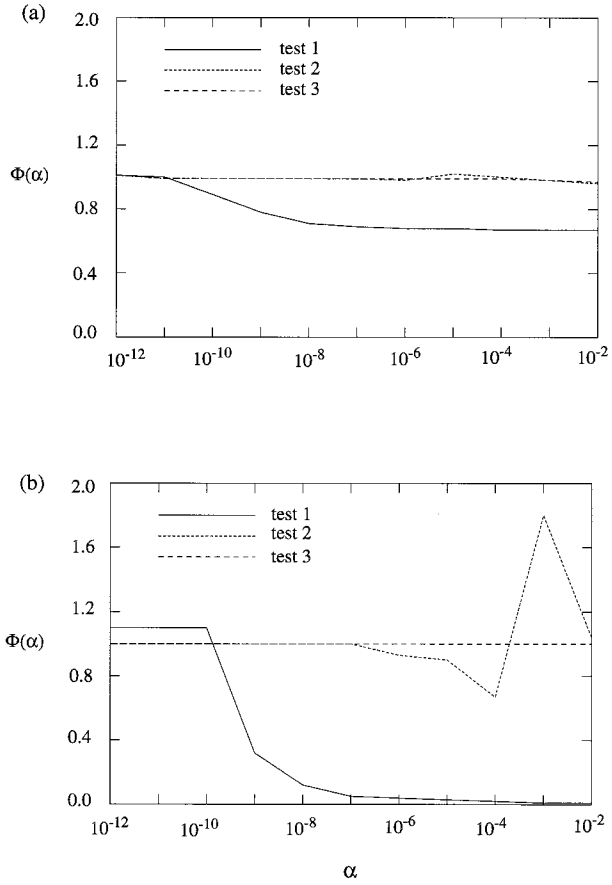

FIG. 1. Plot of function $\Phi(\alpha)$ in (3.18) for vertical velocity (a) and for rainwater mixing ratio (b). The solid curve is for test 1 in which the original parameterization schemes are used, dotted curve for test 2 in which the evaporation of rain follows Eq. (3.14) with q_{ecrit} set to 0.001 g kg^{-1}, and dashed curve for test 3 in which q_{ecrit} is set to 0.1 g kg^{-1}.

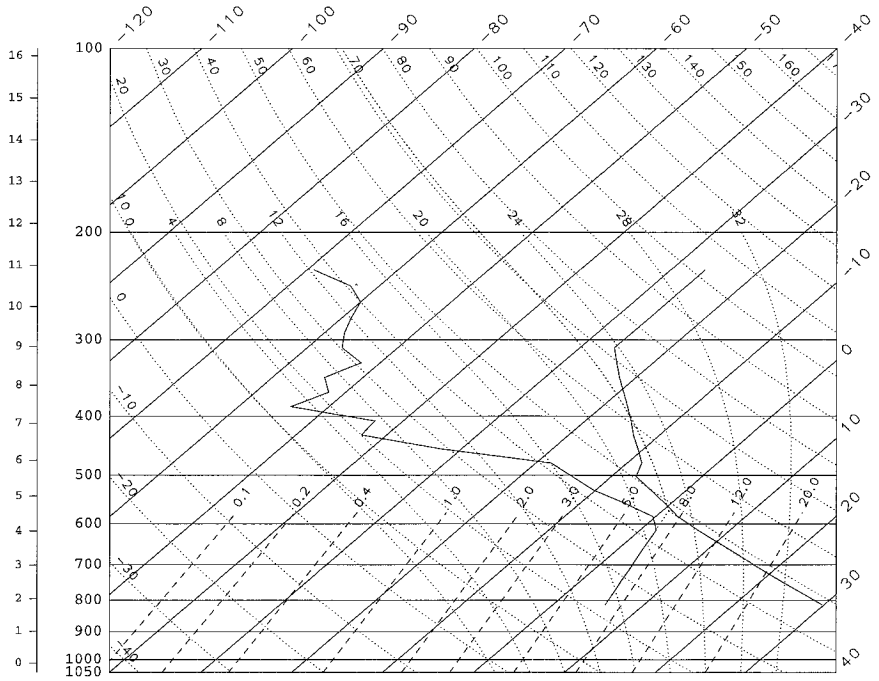

FIG. 2. Skew T diagram depicting initial temperature and moisture profiles.

the domain. We have also examined $\Phi(\alpha)$ for some selected points and found similar results. In both Figs. 1a and 1b, the solid line represents test 1, the dotted line test 2, and the dashed line test 3. Clearly, without the modification of the scheme, the TLM approximates the nonlinear model poorly. The modified scheme (3.14) with $q_{ecrit} = 0.001$ g kg^{-1} results in a much better approximation as long as the perturbation is sufficiently small. As the threshold value is increased to 0.1 g kg^{-1}, $\Phi(\alpha)$ has a uniform value of 1 for α ranging from 10^{-12} to 10^{-2}. These tests indicate that the nonlinearity can be greatly reduced by modifying the original scheme. Although test 3 suggests a better approximation of the TLM to the nonlinear model, we are inclined to choose a scheme that reduces the nonlinearity and meanwhile modifies the physics as little as possible. As mentioned earlier in this section, in 4DVAR the gradient is calculated for an infinitesimal perturbation. As shown in Fig. 1, the modified scheme (3.11) with a threshold value of 0.001 g kg^{-1} is able to provide a good approximation of the TLM to the nonlinear model as long as the perturbations are very small. These tests also indicate that with on/off switches, the TLM can still approximate the nonlinear model very well.

4. Retrieving cloud structure of a simulated storm

a. Control simulation

The control experiment was a simulation of moist convection initiated by a warm, moist bubble. The integration domain was 33.5 km in both horizontal directions and 10 km in the vertical, with grid intervals $\Delta x = \Delta y = 500$ m and $\Delta z = 400$ m. The sounding used for the initial temperature and moisture profiles is shown by the solid lines in Fig. 2. This is a fairly typical preconvective summertime sounding from the Denver region. The initial velocity fields were assumed zero. To initiate convection, a warm, moist bubble was inserted in the center of the domain at a height of 2 km. The initial impulse was 8 km wide and 4 km deep, with a temperature excess of 1°C and moisture excess of 1 g kg^{-1}. We use the Adams–Bashforth time-differencing scheme with a time step of 10 s. The boundary conditions for the velocities normal to the boundaries are assumed zero and, for other variables, their derivatives normal to the boundaries are assumed zero. The eddy viscosity ν was set to 150 m^2 s^{-1}, a typical value used in numerical simulations, and κ was set to 3ν. The modifications of the parameterization schemes described in the last section were not used in the control simulation.

Cloud first started to form in the model at about 17 min when the warm bubble reached the lifting condensation level (about 4 km). The storm was fully developed at about 33 min with a maximum rainwater mixing ratio of ~3 g kg^{-1} and maximum vertical velocity of ~16 m s^{-1}. Figures 3 and 4 show u, w, T', q_v, q_c, and q_r fields in the plane $y = 6$ km (center of the storm) at $t = 29.2$ min and $t = 45.8$ min, respectively (note that the plots do not include the boundary points). The q_c and q_r fields are overlaid with the velocity vector field. It should be noted that T', q_v, and q_c are diagnosed from the prognostic variables θ_l, q_t, and q_r. The storm shown

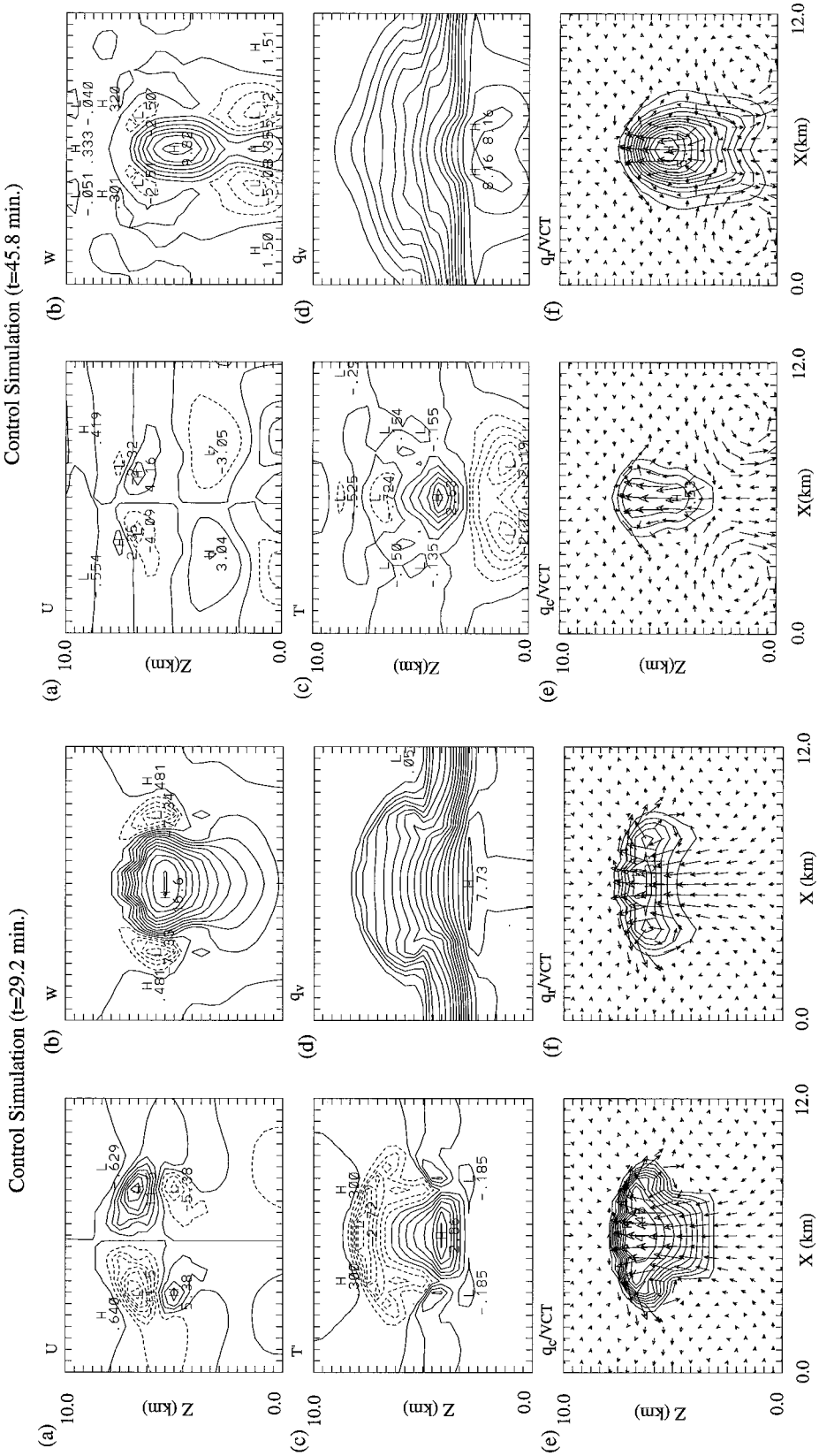

FIG. 3. Vertical cross sections through the center of the storm at $t = 29.2$ min in the control simulation. (a) The x component of horizontal velocity (in m s^{-1}); (b) vertical velocity (in m s^{-1}); (c) perturbation temperature in °C; (d) water vapor mixing ratio (in g kg^{-1}); (e) cloud water mixing ratio (in g kg^{-1}); and (f) rainwater mixing ratio (in g kg^{-1}).

FIG. 4. Same as Fig. 3, but at $t = 45.8$ min.

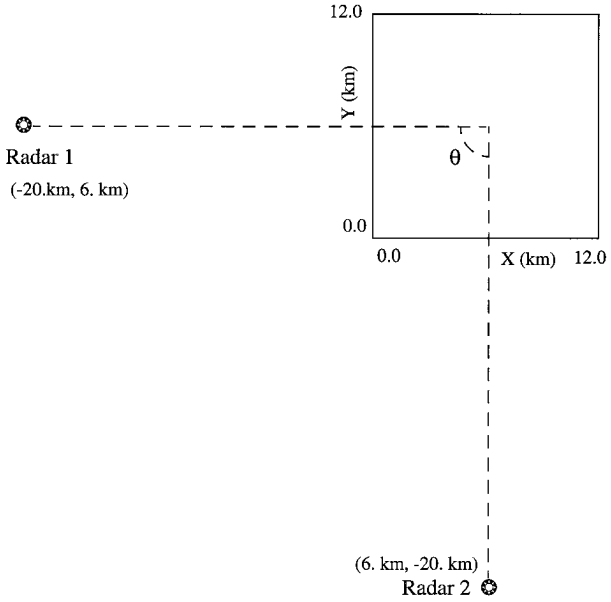

FIG. 5. Locations of the two assumed radars relative to the assimilation domain.

in Fig. 3 is in its developing stage. A mushroom-shaped cloud is formed and the storm is characterized by a strong central updraft. The positive temperature excess is 2.86°C. The negative temperature excess above it is caused by adiabatic cooling. In the dissipating stage of the storm, as shown in Fig. 4, evaporative cooling produces negative temperature perturbations near the ground and drives a downdraft at low levels. The positive buoyancy in the center of the storm is still sustained at this time. The cloud is dissipating and rain is falling to the ground.

In the following sections, the fields shown in Fig. 3 and Fig. 4 will be taken as the actual fields to verify the accuracy of the retrieval.

b. Retrieval experiments and results

In this section, we will test the ability of VDRAS by performing a number of ''identical twin'' experiments. In our experiments, the ''observations'' of radial velocities were constructed using the Cartesian velocity components and rainwater mixing ratio in the control simulation through Eq. (3.5). The ''observations'' of reflectivity were derived from the rainwater mixing ratio in the control simulation using Eq. (3.2) or (3.3). In most of the experiments, we assume two radars are available. The location of the radars relative to the retrieval domain are depicted in Fig. 5. With this geometry, the two radar beams are nearly perpendicular. We have conducted a series of experiments reducing the angle θ (see Fig. 5) up to 20° and found that the dependence of the retrieval on θ is quite small. The retrieval was performed on a domain of $13 \times 13 \times 10$ km^3 with a grid spacing of 500 m in the horizontal and 400 m in the vertical. Although a Doppler radar observes reflectivity, in most of the following experiments, the rainwater mixing ratio that can be estimated using a Z–q_r relation will be used as observational data. That is, the cost function (3.4) is minimized. The problem of directly assimilating reflectivity data will be discussed in a later experiment. For practical reasons, the retrieval experiments were stopped as the cost function leveled out. This generally occurred between 50 and 100 iterations. We will show results using 100 iterations for all experiments presented in this paper. The quality of the retrieval will be assessed by the relative rms error and by comparing the retrieved fields with the actual fields at the end of the assimilation window. The relative rms error is the rms error normalized by the standard deviation of the actual field.

1) RETRIEVING THE CLOUD STRUCTURE AT DIFFERENT STAGES OF THE STORM

Our first two retrieval experiments were intended to examine the performance of the retrieval at different stages of storm development. Experiment A was conducted at the developing stage and experiment B at the dissipating stage of the storm. Both experiments assimilated two sets of data, separated by an interval of 3.33 min. The assimilation window for experiment A was from $t = 25.8$ min to $t = 29.2$ min, and for experiment B from $t = 42.5$ min to $t = 45.8$ min. The input data were radial velocity from two radars and rainwater mixing ratio. The objective in the 4DVAR retrieval experiments is to find an initial state (at $t = 25.8$ min for experiment A and at $t = 42.5$ min for experiment B) that will, upon model integration, produce solutions as close to the observations as possible by minimizing the cost function J_2. Since the quasi-Newton conjugate gradient method used for the minimization is an iterative method, a first guess of the initial state is needed to start the minimization procedure. The first-guess fields for these two experiments and for the rest of the experiments presented in this paper were determined in the same fashion. Zero fields were given to the first-guess fields of the velocities. The first guess of the liquid water potential temperature θ_l and the total water mixing ratio q_t were determined using the mean soundings (shown in Fig. 2) and the rainwater field from the control simulation in the following manner. First, the maximum values in the first-guess fields of θ_l and q_t were determined by taking the difference of the mean values between the surface level and the level at which the rainwater reaches its maximum shown in the soundings. These maximum values were estimated in such a manner because θ_l and q_t are both conserved variables as long as the rainwater remains in the rising parcel. These maxima were then multiplied by $q_r(x, y, z)/q_{r\max}$ to yield their first-guess fields where $q_{r\max}$ is the maximum value in the rainwater mixing ratio field. Once the first guess of q_t and θ_l is provided, the perturbation temperature T',

cloud water mixing ratio q_c, and water vapor mixing ratio q_v can be computed through the diagnostic relations described in section 2. Figure 6 shows the first-guess fields of T', q_c, and q_v for both experiments.

Starting from the first-guess fields described above, the retrieval experiments were carried out by minimizing the cost function J_2 with the penalty and background terms excluded. During the minimization process, the modified scheme for evaporation of rain was used in place of the original scheme, and the modified scheme for rainwater terminal velocity was used in the calculation of $V_{r,i}$ [see Eq. (3.5)] in the cost function but not in the precipitation process [see Eqs. (2.6), (2.8), and (2.9)]. Figures 7 and 8 present the retrieved fields at the end of the assimilation window from experiment A and experiment B, respectively. The relative rms error is shown at the top of each plotted field. Comparing the retrieved fields with their corresponding actual fields shown in Figs. 3 and 4, one can see that, for both experiments, the discrepancies are very small except for the perturbation temperature field. At the storm dissipating time, however, the retrieved temperature field has much smaller error than at the developing time. It is interesting to note that the relative error in retrieved liquid water potential temperature field θ_l is not large, about 2.3% in both experiments. However, the actual temperature has a much larger relative error. Further examination revealed that the absolute errors in θ_l and in T' were the same order and the large difference in their relative errors was caused by the difference of the standard deviations in these two fields.

The reason why a better temperature retrieval was obtained at the dissipating stage of the storm is explained as follows. Part of the retrieved temperature perturbation is necessary to balance the waterloading due to cloud and rain. Since the cloud and rainwater fields are retrieved quite accurately, this part of the temperature perturbation is also retrieved accurately. Therefore, since the amount of rainwater is greater in the dissipating stage of the storm, the temperature retrieval is more accurate at this stage.

2) ADDING BACKGROUND TERM

The objective of 4D data assimilation is to fit a model solution to observations as closely as possible. However, observations of the atmosphere are often sparse and spaced much farther apart than the grid points. On the convective scale, radar data is generally available at very fine resolution; however, these observations are often concentrated in small areas and there are no observations with a comparable resolution outside these regions. When the observations are incomplete, other types of observations or some a priori information need to be incorporated by adding a background term to the cost function. The general form of the background term has been given in Eq. (3.6). On the large scale, some dynamic balance is often used to provide background information (e.g., Heckley et al. 1992). On our scale of interest, however, simple balance equations are not available. Therefore our focus will be on incorporation of data from other sources to fill the data-void region. Since these data usually have much less resolution than the radar data, they are considered here as background data. One simple application of adding other data to the cost function is the use of mean properties observed before the convection developed. The background term can be written as

$$J_b = \sum_{\sigma,\tau,m} \eta_{x_m}(x_m - \overline{x_m})^2, \tag{4.1}$$

where x_m represents any model variable and $\overline{x_m}$ is the mean profile of this variable. The quantity η_{x_m} is the weighting constant. It is zero in the data-rich region and has a specified value in the region of vanishing radar echoes. This specification of η_{x_m} reduces the error covariance matrix B into a diagonal matrix. Preliminary experiments with real data have shown that this background term is very important in keeping the wind outside the convection close to the mean profile, meanwhile fitting the cloud model to radar observations within the convection (Sun et al. 1995; Sun and Crook 1995). In the current study with simulated data, since we have data everywhere in the domain, this term will not play as important a role as with real data. However, we still expect this term can add information to the variable least constrained by the available radar data, for instance, the temperature field. To examine the effect of this background term on the quality of the retrieved temperature field, experiments A and B were repeated with a background term added to the cost function. The background term used in these two experiments is

$$J_b = \sum_{\sigma,\tau} \eta_T T'^2. \tag{4.2}$$

Note that T' is the perturbation temperature and its mean value is zero. Here, η_T is zero if q_r is greater than 0.01 g kg^{-1} and 0.1 for other values of q_r. With this background term, the retrieved temperature fields in both experiments were improved. The relative rms errors were reduced from 45.2% to 38.2% in the developing stage and from 25.0% to 12.3% in the dissipating stage. Figure 9 compares the actual temperature field with the retrieved temperature fields with (Fig. 9c) and without (Fig. 9b) the background term (4.2) at the dissipating stage. It is seen that some background noise is removed and the positive temperature excess is closer to that in the actual field after the background term is applied.

3) RETRIEVAL USING SINGLE RADAR INFORMATION

Extracting information from single-Doppler radars has attracted a great deal of attention in recent years. Various techniques have been developed to determine the 3D wind and temperature fields from single-Doppler observations of the dry boundary layer. However, re-

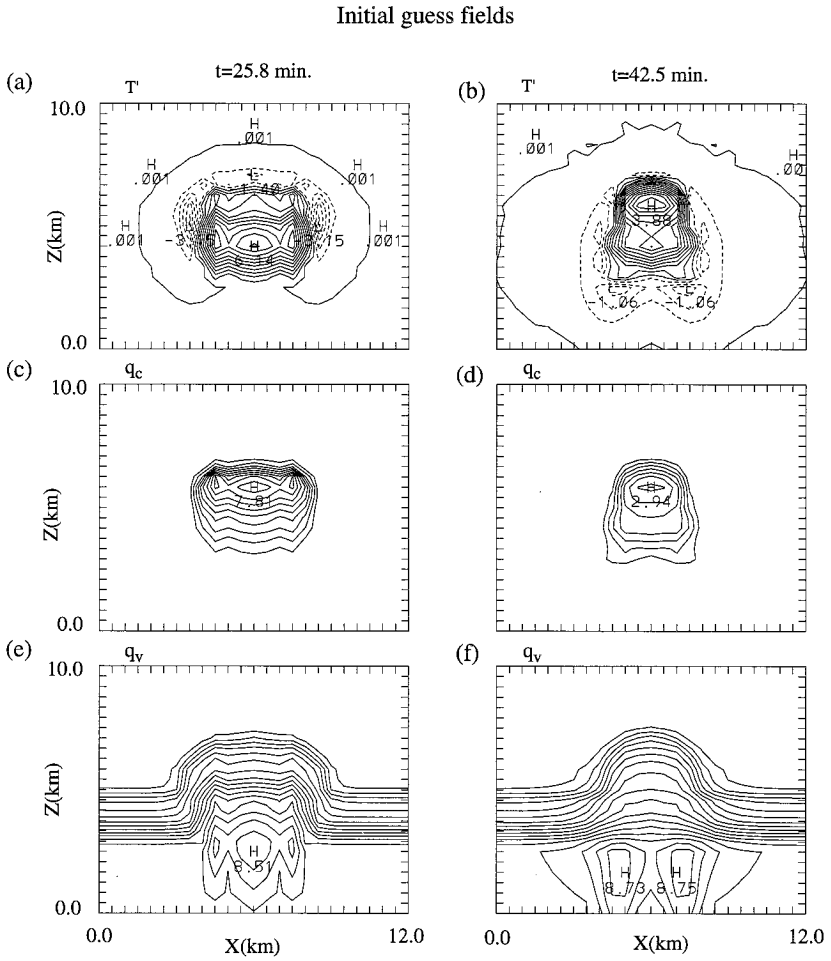

FIG. 6. First-guess fields of perturbation temperature [(a) and (b)], cloud water mixing ratio [(c) and (d)], and water vapor mixing ratio [(e) and (f)]. (a), (c), and (e) are at $t = 25.8$ min. (b), (d), and (f) are at $t = 42.5$ min.

trieving unobserved variables in a convective storm from single-Doppler data is far more challenging than in the boundary layer due to the presence of moist processes. In principle, VDRAS can be used to derive information from a single-Doppler radar. However, how much information can be obtained from single-Doppler observations is a question that needs to be answered.

When observations from one radar are used, it is necessary to include the penalty term and the background term in the cost function to supplement the data inadequacy. Experiments at the developing stage and the dissipating stage both suggested that the inclusion of these terms helped obtain a more accurate retrieval. Figure 10 shows the retrieved fields at $t = 45.8$ min from the experiment using single radar information. This experiment was similar to experiment B but used radial velocity data only from radar 1. The other differences from experiment B were the implementation of the temporal and spatial smoothness penalty functions and the background term (4.2) in this experiment. It can be observed from the figure that the main structures of the storm are captured. However, some discrepancies in terms of magnitude are noticeable. Compared with the experiment with data from two radars, the relative rms error in the thermodynamical and microphysical fields changed very little. The error in the velocity fields increased rather substantially, from 0.5% to 12.3% for the horizontal velocity and from 0.9% to 9.1% for the vertical velocity.

4) ASSIMILATING REFLECTIVITY DIRECTLY

In the above experiments, we used rainwater mixing ratio, which could be obtained through a Z–q_r relation, as input data. We can also assimilate reflectivity data directly. In this case, the cost function J_1 is used. Unlike the cost function J_2 in which q_r is a direct model variable, here the reflectivity Z in the cost function is related to q_r through the Z–q_r relation (3.2) if Z is in units of mm^6 m^{-3} or (3.3) if Z is in units of dBZ. Two experi-

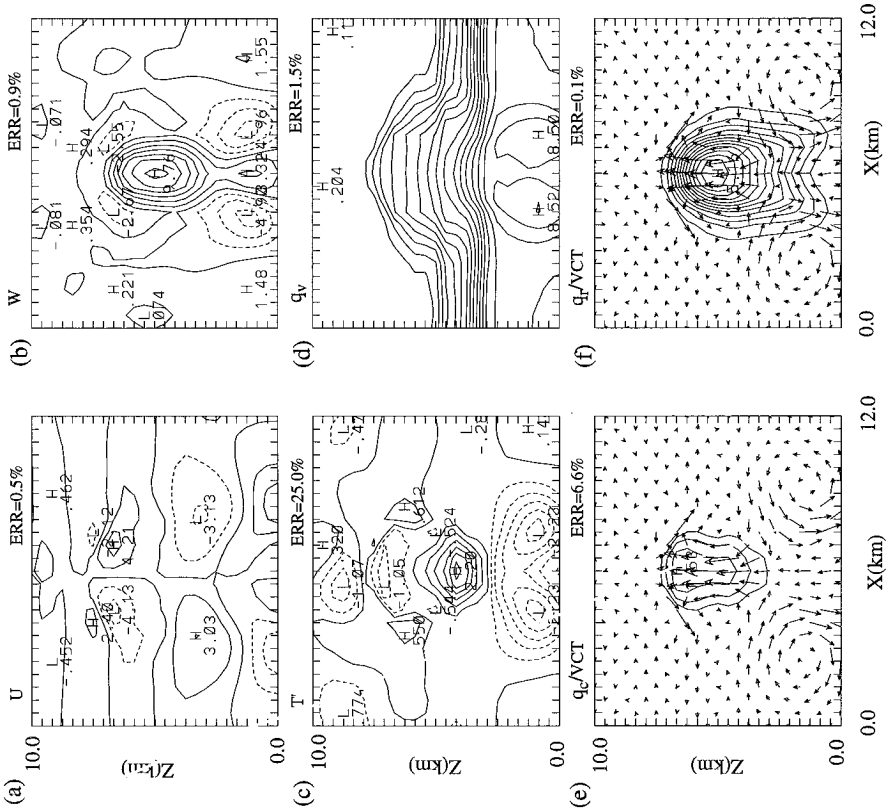

FIG. 7. Vertical cross sections of retrieved fields through the center of the storm at t = 29.2 min in experiment A. (a) The x component of horizontal velocity (in m s^{-1}); (b) vertical velocity (in m s^{1}); (c) perturbation temperature (in °C); (d) water vapor mixing ratio (in g kg^{-1}); (e) cloud water mixing ratio (in g kg^{-1}); and (f) rainwater mixing ratio (in g kg^{-1}).

FIG. 8. Similar to Fig. 7, but at t = 45.8 from experiment B.

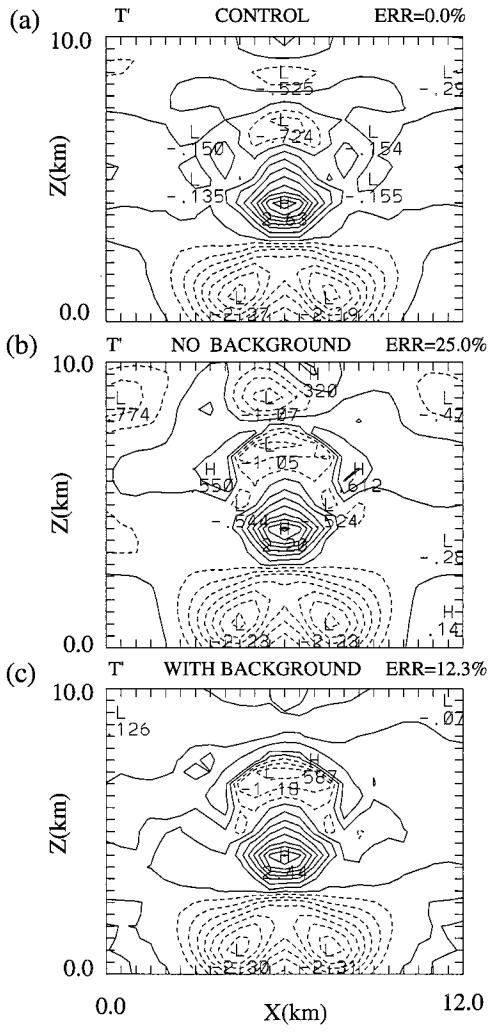

FIG. 9. Vertical cross section of the perturbation temperature field at $t = 45.8$ min from control simulation (a), from experiment B without the background term (b), and from the experiment with the background term (c).

ments were conducted to examine the performance of the retrieval when the reflectivity data were used directly in the cost function. In the first experiment, we assumed the reflectivity data were in units of $mm^6\ m^{-3}$ [Eq. (3.2)]. Since the typical value of Z is a few orders larger than that of the velocity, the value of the weighting coefficient η_z must be properly chosen such that the two terms in the cost function (3.1) will have a similar magnitude. Based on this principle, η_z was set to 10^{-4} while η_v was set to 1. The retrieval results from this experiment (not shown) indicated that the error in all of the retrieved fields had a slight increase as compared with the experiment in which the cost function (3.4) was minimized. We also found that when the reflectivity contains error, as will be discussed later in this paper, the degradation by using the cost function J_1 is more prominent.

In the second experiment, the reflectivity was assumed to be in units of dBZ. That is, Z in the cost function is related to q_r through the Z–q_r relation (3.3). The advantage of using reflectivity in units of dBZ is that it typically has values similar to that of radial velocity. However, it was found that the minimization had difficulty converging. This difficulty was caused by the large gradient of the cost function associated with very small q_r as explained in the following. When taking the derivative with respect to q_r in the adjoint model, the second term in the cost function (3.1) will lead to the following variation:

$$\delta J_1 = \cdots + 2\rho_z(Z - Z_i^{ob}) \times \frac{17.5}{\rho q_r \mathrm{Ln}10}\delta q_r + \cdots \cdot \quad (4.3)$$

The variable q_r appears in the denominator, which will result in a very large gradient when q_r is small. One way to circumvent this problem is to set the term in (4.3) to zero if q_r is less than a specified value q_{rc} meaning that the data are not assimilated when they are smaller than q_{rc}. Since we want to keep as much data as possible, a small value of q_{rc} is desirable. Several experiments were conducted to determine the best value for q_{rc} and it was found that it could not be smaller than 0.1 g kg^{-1}. The experiment with reflectivity as input data and $q_{rc} = 0.1$ g kg^{-1} shows that the retrieved fields are quite close to those in the experiments that assimilate q_r except for the q_r field. In Fig. 11, we compare the retrieved q_r field from the experiment in which J_1 is minimized with the retrieved field from experiment A (in which J_2 is minimized) and the actual field at $t = 29.2$ min. It is observed that the retrieved q_r field has some substantial difference from the actual field. Its relative rms error is 20.7%, much larger than that from experiment A, which is only 0.7%. It should be noted, however, that most of this error is distributed in the region where the rainwater mixing ratio is smaller than q_{rc} (0.1 g kg^{-1}).

5) SENSITIVITY TO Z–q_r RELATION

The Z–q_r relation (3.2) used in this study was derived by assuming the Marshall–Palmer drop-size distribution. In practice, various empirical Z–q_r relations have been used. It is natural to ask how sensitive the retrieval is to variation in the Z–q_r relation. To answer this question, an experiment was conducted using a different rainwater mixing ratio field as the input data. Taking the reflectivity field derived from Eq. (3.2) as the actual or observed reflectivity, a new q_r can be obtained by using an empirical Z–q_r relation

$$Z = 2.4 \times 10^4\ \rho q_r^{1.82}. \quad (4.4)$$

Equation (4.4) is obtained by eliminating the rainfall rate between the Marshall–Palmer expressions for the Z–R and q_r–R relationships (Battan 1973). The q_r field computed from (4.4) contains an error from 15% to 32% for q_r ranging from 1 to 5 g kg^{-1}. Experiments were conducted with these perturbed q_r input data at both the developing stage and the dissipating stage. The back-

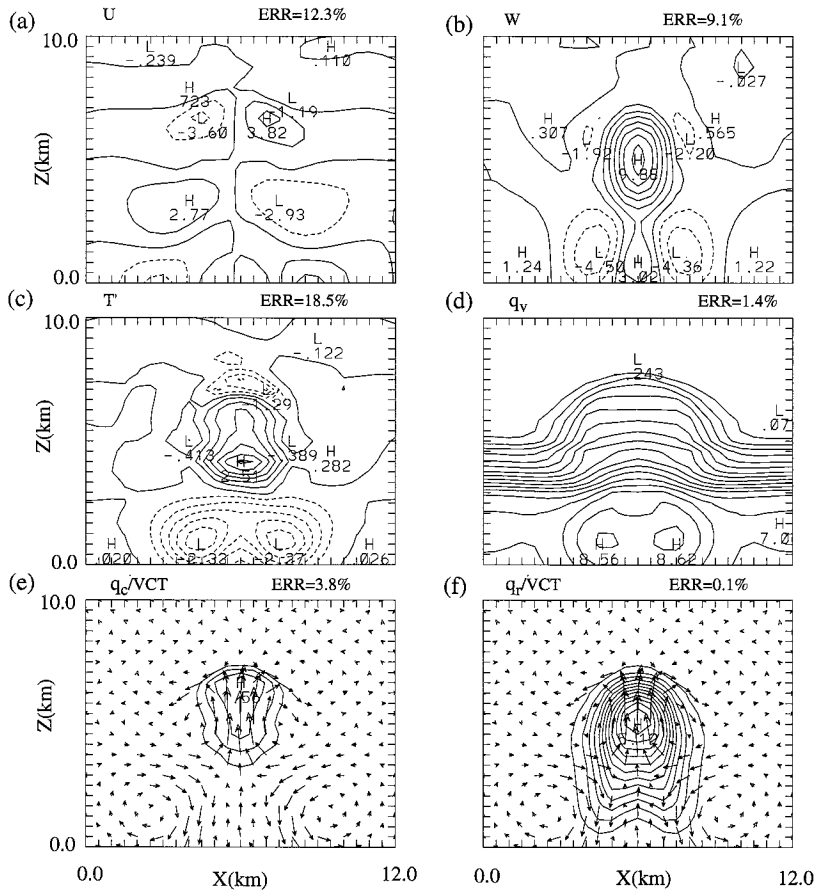

FIG. 10. Similar to Fig. 7, but from the experiment with only one radar information.

ground term (4.2) was included in these experiments. Except for the q_r and T' fields, the retrieved fields showed very little change compared with their corresponding experiments in which the exact q_r was used. At the developing stage, the temperature retrieval was also affected very little by the inaccurate q_r data, while the error in the retrieved temperature field increased from 12.3% to 28% at the dissipating stage. This is partly due to the fact that more error was added to the q_r field at the dissipating stage because q_r has greater magnitude at that time. Another reason is that the temperature retrieval is more dependent on the q_r data at the dissipating stage. The retrieved temperature field and q_r field at the dissipating stage are shown in Fig. 12 and compared with their actual fields.

6) SENSITIVITY TO MOIST PROCESSES

The parameterized moist processes contain several constants that are empirically determined. In order to investigate the impact of the moist processes on the retrieval, several retrieval experiments were conducted by alternately neglecting some of the moist processes. At the developing stage, the neglect of either the accretion or the autoconversion process mainly affected the rainwater field with the relative rms error increasing from 0.7% to 4.8% and 7.0% respectively. The error in the cloud water field increased slightly and in the other fields remained the same. The neglect of the accretion process at the dissipating stage had a strong influence on both the rainwater and the cloud water fields and a slight influence on the perturbation temperature field. Figure 13 shows the retrieved fields of q_c and q_r. The cloud water content is twice that in the actual field and the rainwater content decreases substantially. In the next experiment, we tested the sensitivity to the precipitation process by assuming zero fall velocity. As the fall velocity was set to zero, the radial velocity was overestimated. In this case, not only the microphysical and thermodynamical retrieval but also the velocity retrieval were affected. Figure 14 displays the retrieved fields from the experiment with zero fall velocity. It is shown that both the cloud water and the central vertical velocity are overestimated and the downdrafts are underestimated. The rain remains in the upper levels. Another experiment to test the sensitivity to the precipitation process was conducted by changing the exponential value in Eq. (2.16) from 0.125 to 0.2. The results show an

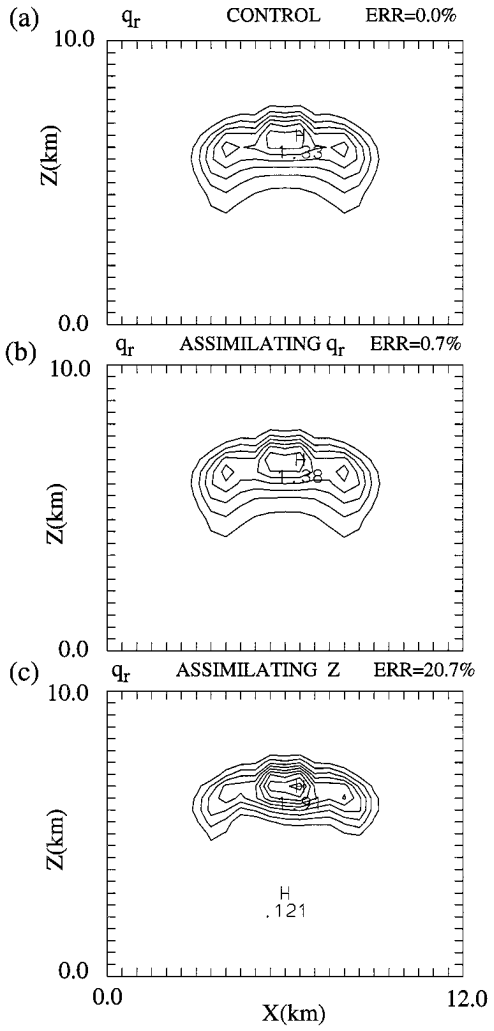

FIG. 11. Vertical cross section of the retrieved rainwater mixing ratio at $t = 29.2$ min from control simulation (a), from experiment A assimilating the rainwater mixing ratio (b), and from the experiment directly assimilating reflectivity (c).

increase in relative rms errors with a similar magnitude for all of the retrieved fields.

The above experiments indicate that the retrieval of cloud water and rainwater are rather sensitive to some of the physical parameterization constants. A possible method for determining more accurate constants is to treat them as control variables so that they can be adjusted in a similar fashion to the initial conditions. However, an effort to ''tune'' these parameters by including them as control variables turned out to be unsuccessful. A possible explanation for this lack of success is that the data are insufficient to uniquely define solutions of the parameters in moist physics. Therefore, it is important to implement good physical parameterization schemes in order to obtain a reliable microphysical retrieval.

7) SENSITIVITY TO OBSERVATIONAL ERRORS

In the above experiments, we have assumed that the radial velocity and reflectivity data were error free. In reality, however, observations can contain various errors. In this section, we test the sensitivity of the retrieval to observational errors, in particular, random noise in radial velocity and calibration error in reflectivity. To examine the performance of the retrieval with random noise in radial velocity, an experiment was conducted by adding a 20% random error to the radial velocity data from both radars, namely, $v_{re} = v_r(1 + 0.2e)$, where e represents the random error field in the range of ± 1. Results from this experiment showed that the relative errors in the retrieved velocity fields increased slightly, from 0.63% and 1.1% to 1.6% and 4.1% for the horizontal components and the vertical component, respectively, while the changes in the other fields were negligibly small.

The calibration error in reflectivity typically ranges from 1 to 3 dBZ. In order to test the sensitivity of the retrieval to reflectivity calibration error, we added a 3-dBZ error to the reflectivity data and then tested the performance of the retrieval. It was found that the retrieved fields of T', q_c, and q_r were rather sensitive to the calibration error while the other fields had very little change. In Fig. 15, we display the retrieved fields of T', q_c, and q_r (the right three panels) and compare them with the retrieval with error-free data (the left three panels). As a result of the 3-dBZ calibration error, the rainwater mixing ratio is increased by more than 2 g kg^{-1}, which consequently produces errors in the perturbation temperature and the cloud water.

The above experiments indicate that the 4DVAR retrieval technique can tolerate random velocity errors better than reflectivity calibration errors. Although larger sensitivity was found in the latter experiment, the main structure of the storm was still captured. From this point of view, the technique is quite robust to both types of observation errors.

5. Summary and discussions

In this paper, a variational Doppler radar analysis system (VDRAS) was described. The basic components of VDRAS include a forward cloud model with warm rain parameterization and its adjoint. The ability of VDRAS in determining the dynamical and microphysical variables within convective storms was examined through a series of identical-twin experiments. These experiments demonstrated that detailed cloud structures in a convective storm could be retrieved by fitting the numerical model to radial velocity and rainwater data using information from dual- or single-Doppler radars. The experiments also demonstrated that the adjoint model developed by keeping the on/off switches the same as in the basic state did not cause any problem in the minimization procedure. The problems of high nonlinearity

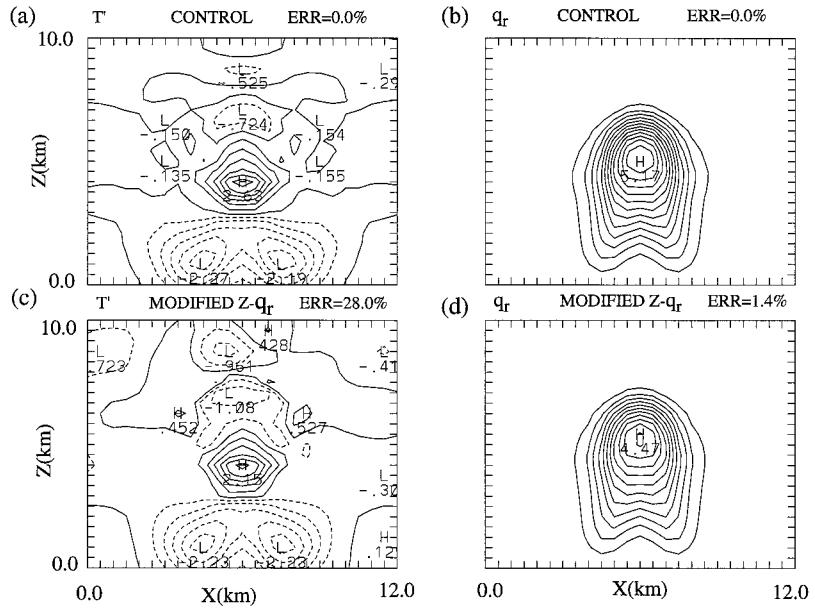

FIG. 12. Vertical cross sections of perturbation temperature [(a) and (c)] and rainwater mixing ratio [(b) and (d)] at $t = 45.8$ min. (a) and (b) are from the control simulation and (c) and (d) are from the experiment in which a different Z–q_r relation (4.6) is used.

associated with some of the physical processes could be avoided by slightly modifying the schemes.

It was also found that assimilating rainwater mixing ratio obtained from the reflectivity data using a Z–q_r relation resulted in a better performance of the retrieval procedure compared to direct assimilation of reflectivity. When the reflectivity data in units of dBZ were directly assimilated, the nonlinearity introduced to the cost function through the highly nonlinear Z–q_r relation could cause problems in the minimization procedure. Since any Z–q_r relation contains approximations, we varied the constants in the Z–q_r relation to test the sensitivity of the retrieval to these variations. It was shown that the retrieval was rather robust to the error caused by the change in the Z–q_r relation.

Retrieval of the temperature field presented more

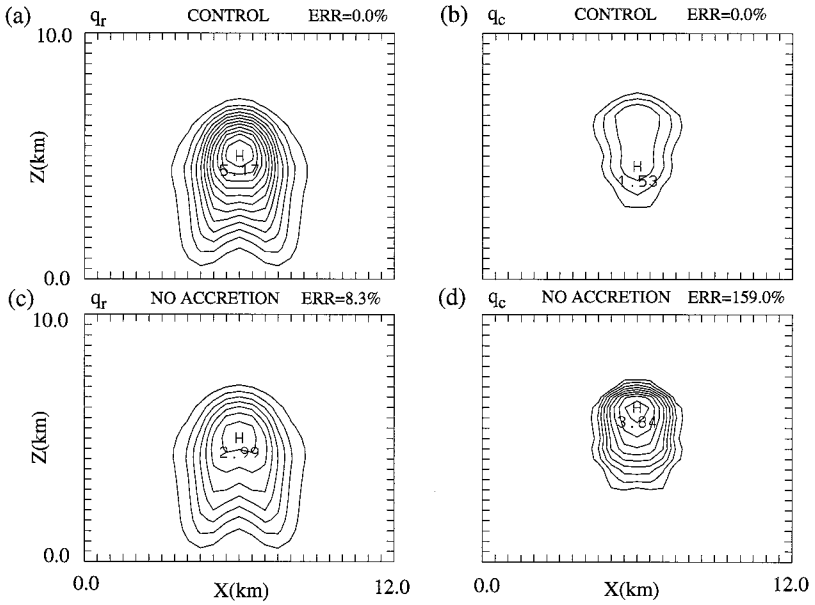

FIG. 13. Comparison of the retrieved rainwater mixing ratio (c) and cloud water mixing ratio (d) from the experiment in which the accretion process is neglected with their actual fields [(a) and (b)] at $t = 45.8$ min.

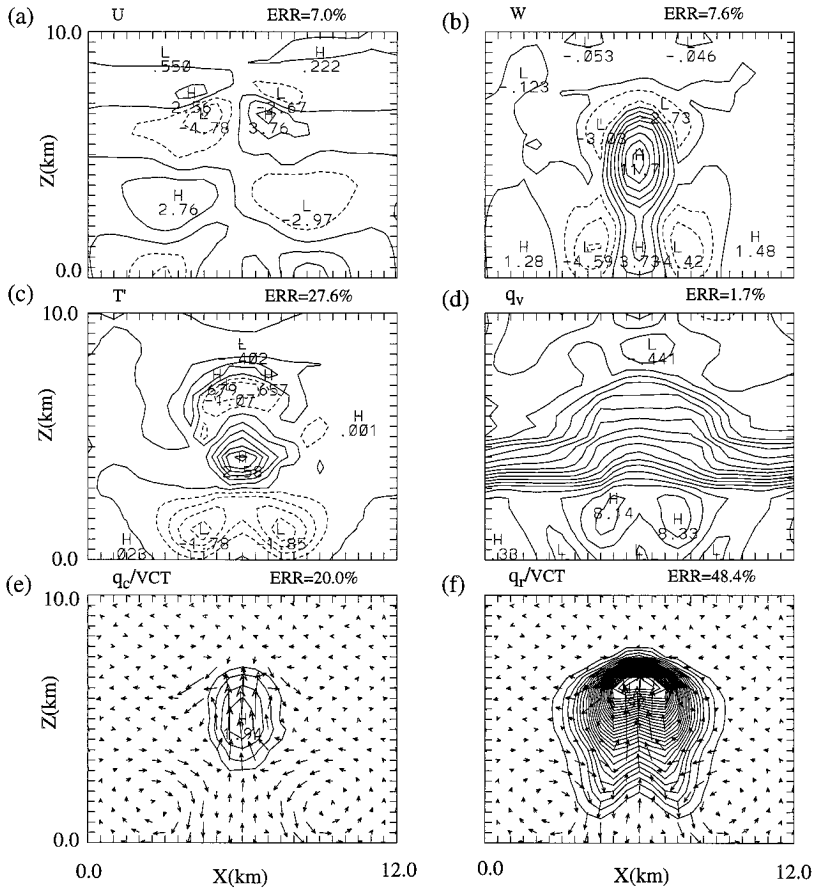

FIG. 14. Similar to Fig. 7, but from the experiment in which the rainwater fall velocity is assumed zero.

challenges compared to that of other variables in the model, especially in the initial developing stage of the storm. Although the inclusion of a background term based on the environmental temperature helped reduce the error, the error in the temperature retrieval remained the largest. It is obvious that more information is needed to improve the temperature retrieval. This information could be some additional constraints based on physical plausibility or observations from other sources, for instance, aircraft or surface mesonet data. Unfortunately, these data are not generally available except for some specially designed field experiments.

When only single-Doppler information was provided, the retrieved thermal and microphysical fields were slightly degraded. Although the error in the retrieved velocity fields increased noticeably, their structures were retrieved reasonably well. If the model accurately represents the atmosphere, then the retrieval technique is quite powerful in differentiating the water vapor, cloud water, and rainwater even with observations from only one radar. However, the experiments in which the parameters of some physical processes were neglected suggested that poor representation of a moist process could have a large impact on the retrieval of the microphysical fields. Attempts to tune these parameters did not show any success with the amount of available data. Therefore, it is important to implement good physical parameterization schemes in order to obtain a reliable microphysical retrieval.

VDRAS was also tested on radial velocity data with a 20% random error and reflectivity data with a 3-dBZ uniform error (to mimic calibration errors), respectively. Results suggested that the technique was able to retrieve the general structure of the storm when the data contained errors at those magnitudes. However, the retrieval was more sensitive to the reflectivity calibration error than to the random noise in the radial velocity fields. In these experiments, the error statistics were not used to determine the error covariance matrix in the cost function due to the difficulty in calculating the inverse matrix. For simplicity, a constant diagonal matrix was used to approximate the error covariance matrix. In the current simulated data study, this approximation did not appear to affect the retrieval results to a great extent. However, better approximations may be required to successfully assimilate observational data.

In the second part of this two-part paper, VDRAS will be applied to real observations of convective storms.

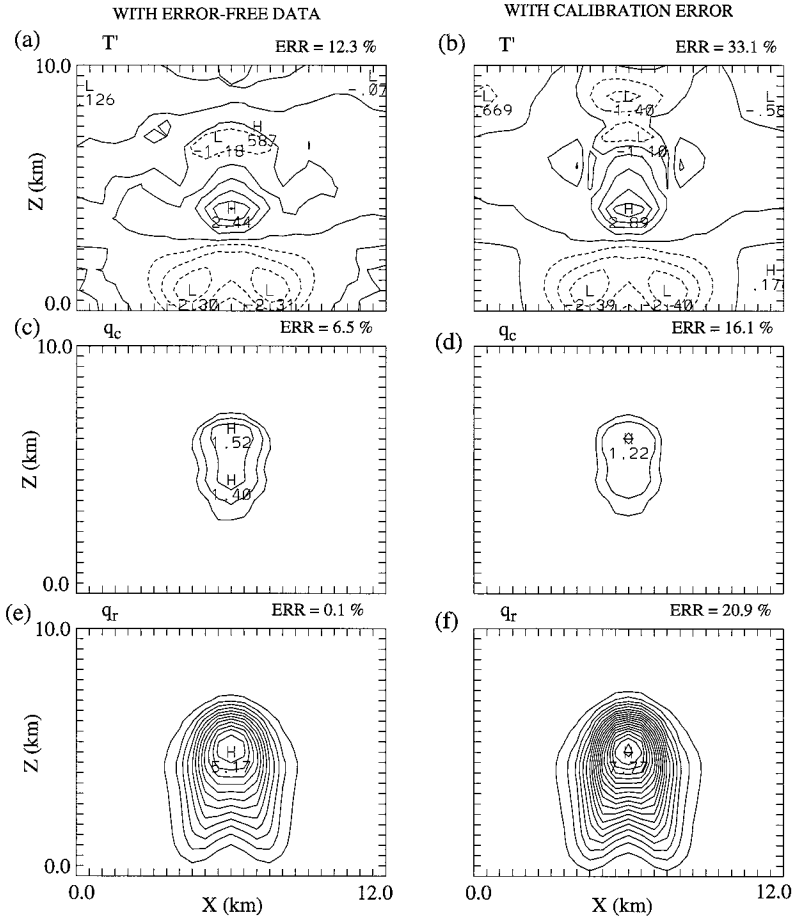

FIG. 15. Vertical cross section of perturbation temperature [(a) and (b)], cloud water mixing ratio [(c) and (d)], and rainwater mixing ratio [(e) and (f)]. The left column is for the experiment with error-free data and the right column is for the experiment with calibration error.

Although in the current paper we have showed that VDRAS was able to handle certain errors in the input data, the observational data will provide the truest test of the retrieval scheme. Another important issue that can be addressed by experiments with real data will be the model's representativeness to the motion in the atmosphere. Preliminary study with some real data has shown promise (Sun et al. 1995; Sun and Crook 1995). Further analyses and verification by aircraft observations will be presented in Part II of this paper.

Acknowledgments. This research is sponsored by the National Science Foundation through an Interagency Agreement in response to requirements and funding by the Federal Aviation Administration's Aviation Weather Development Program. The views expressed are those of the authors and do not necessarily represent the official policy or position of the U.S. government. The authors are grateful to Dr. Johannes Verlinde for his contribution in coding of some of the moisture parameterization schemes. Thanks are also due to Drs. Xiaolei Zou and Chris Davis for review of this paper.

APPENDIX

Calculating the Gradient of the Cost Function Using the Adjoint Model

The numerical model described in section 2 can be represented in vector form as

$$\frac{\partial \mathbf{x}}{\partial t} = F(\mathbf{x}), \qquad \mathbf{x}(t_0) = \mathbf{x}_0. \tag{A.1}$$

The vector x contains the six prognostic variables (u, v, w, θ_l, q_r, q_t). The discretized form of (A.1) can be written as

$$\mathbf{x}(t_n) = F_n(\mathbf{x})\mathbf{x}(t_0), \tag{A.2}$$

where $\mathbf{x}(t_n)$ represents the model forecast at time t_n and

$\mathbf{x}(t_0)$ the initial conditions of the prognostic variables. Here, $F_n(x)$ denotes the operator matrix to obtain $\mathbf{x}(t_n)$ from the initial condition $\mathbf{x}(t_0)$.

Let $\delta\mathbf{x}(t_n)$ denote the first-order variation of $\mathbf{x}(t_n)$ resulting from the perturbation $\delta\mathbf{x}(t_0)$, then the tangent linear model (TLM) of (A.2) can be written as

$$\delta\mathbf{x}(t_n) = G_n(\mathbf{x})\delta\mathbf{x}(t_0), \tag{A.3}$$

where $G_n(\mathbf{x})$ is the linear operator of the TLM. The adjoint model can be obtained by taking the transpose of the tangent linear model, that is,

$$\delta\mathbf{x}'(t_0) = G_n^T(\mathbf{x})\delta\mathbf{x}'(t_n), \tag{A.4}$$

where $\delta x'$ represents the adjoint variable and $G_n^T(\mathbf{x})$ is the operator of the adjoint model. As shown by Talagrand and Courtier (1987), the inhomogeneous adjoint equation is constructed by adding a forcing term to (A.4), that is

$$\delta\mathbf{x}'(t_0) = G_n^T(\mathbf{x})\delta\mathbf{x}'(t_n) + \nabla H(\mathbf{x})\delta t, \tag{A.5}$$

where $H(x)$ represents the integrand of the cost function (3.1) or (3.4) and ∇ represents differentiation with respect to x. Talagrand and Courtier (1987) showed that the final result $\delta\mathbf{x}'(t_0)$ obtained from (3.11) is equal to the gradient of the cost function with respect to the IC.

The adjoint model represented by Eq. (A.5) contains six prognostic equations. The prognostic variables in these equations are the sensitivities or the gradients of the cost function with respect to their corresponding prognostic model variables.

REFERENCES

Armijo, L., 1969: A theory for the determination of wind and precipitation velocities with Doppler radar. *J. Atmos. Sci.*, **26,** 570–573.

Bao, J. W., and T. T. Warner, 1993: Treatment of on/off switches in the adjoint method: FDDA experiments with a simple model. *Tellus,* **45A,** 525–538.

——, and Y.-H. Kuo, 1995: On–off switches in the adjoint method: Step functions. *Mon. Wea. Rev.,* **123,** 1589–1594.

Battan, L. J., 1973: *Radar Observation of the Atmosphere.* University of Chicago Press, 324 pp.

Courtier, P., 1985: Experiments in data assimilation using the adjoint model technique. Preprints, *Workshop on High-Resolution Analysis,* Reading, United Kingdom, European Centre for Medium-Range Weather Forecasts, 1–20.

Derber, J. C., 1985: The variational 4-D assimilation of analyses using filtered models as constraints. Ph.D. dissertation, University of Wisconsin—Madison, 142 pp.

Douady, D., and O. Talagrand, 1990: The impact threshold process on variational assimilation. Preprints, *WMO Int. Symp. on Assimilation of Observations in Meteorology and Oceanography,* Clermont-Ferrand, France, World Meteor. Org., 486–487.

Gal-Chen, T., 1978: A method for the initialization of the anelastic equations: Implications for matching models with observations. *Mon. Wea. Rev.,* **106,** 587–606.

Gill, P. E., W. Murray, and M. H. Wright, 1981: *Practical Optimization.* Academic Press, 401 pp.

Hane, C. E., and B. C. Scott, 1978: Temperature and pressure perturbations within convective clouds derived from detailed air motion information: Preliminary testing. *Mon. Wea. Rev.,* **106,** 654–661.

——, R. B. Wilhelmson, and T. Gal-Chen, 1981: Retrieval of thermodynamic variables within deep convective clouds: Experiments in three dimensions. *Mon. Wea. Rev.,* **109,** 564–576.

Hauser, D., and P. Amayenc, 1986: Retrieval of cloud water and water vapor contents from Doppler radar data in a tropical squall line. *J. Atmos. Sci.,* **43,** 823–838.

Heckley, W. A., P. Courtier, J. Pailleux, and E. Andersson, 1992: The ECMWF variational analysis: General formulation and use of background information. Preprints, *Workshop on Variational Assimilation, with Special Emphasis on Three-Dimensional Aspects,* Reading, United Kingdom, European Centre for Medium-Range Weather Forecasts, 49–94.

Kessler, E., 1969: *On the Distribution and Continuity of Water Substance in Atmospheric Circulation. Meteor. Monogr.,* No. 32, Amer. Meteor. Soc., 84 pp.

Laroche, S., and I. Zawadsky, 1994: A variational analysis method for the retrieval of three-dimentional wind field from single-Doppler data. *J. Atmos. Sci.,* **51,** 2664–2682.

Le Dimet, F. X., 1982: A general formalism of variational analysis. CIMMS Rep. 22, 1–34. [Available from Sarkeys Energy Center, Rm 1110, University of Oklahoma, Norman, OK 73019.]

——, and O. Talagrand, 1986: Variational algorithms for analysis and assimilation of meteorological observations: Theoretical aspects. *Tellus,* **38A,** 97–110.

Lewis, J. M., and J. C. Derber, 1985: The use of adjoint equation to solve a variational adjustment problem with advective constraints. *Tellus,* **37A,** 309–322.

Liu, D. C., and J. Nocedal, 1989: On the limited memory BFGS method for large scale optimization. *Math. Programming,* **45,** 503–528.

Miller, M. J., and R. P. Pearce, 1974: A three-dimentional primitive equation model of cumulonimbus convection. *Quart. J. Roy. Meteor. Soc.,* **100,** 133–154.

Navon, I. M., X. Zou, J. Derber, and J. Sela, 1992: Variational data assimilation with an adiabatic version of the NMC spectral model. *Mon. Wea. Rev.,* **120,** 1433–1446.

Qiu, C. J., and Q. Xu, 1992: A simple adjoint method of wind analysis for single-Doppler data. *J. Atmos. Oceanic Technol.* **9,** 588–598.

Roux, F., 1985: Retrieval of thermodynamic fields from mutiple-Doppler radar data using the equations of motion and the thermodynamic equation. *Mon. Wea. Rev.,* **113,** 2142–2157.

Rutledge, S. A., and P. V. Hobbs, 1983: The mesoscale and microscale structure and organization of clouds and precipitation in midlatitude cyclone. VIII: A model for the ''seeder-feeder'' process in warm-frontal rainbands. *J. Atmos. Sci.,* **40,** 1185–1206.

——, and ——, 1984: The mesoscale and microscale structure and organization of clouds and precipitation in mid-latitude cyclone. XII: A diagnostic modeling study of precipitation development in narrow cold-frontal rainbands. *J. Atmos. Sci.,* **41,** 2949–2972.

Shapiro, A., E. Ellis, and J. Shaw, 1995: Single-Doppler velocity retrievals with Phoenix II data: Clear air and microburst retrievals in one planetary boundary layer. *J. Atmos. Sci.,* **52,** 1265–1287.

Sun, J., and N. A. Crook, 1994: Wind and thermodynamic retrieval from single-Doppler measurements of a gust front observed during Phoenix II. *Mon Wea Rev.,* **122,** 1075–1091.

——, and ——, 1995: Retrieval of the dynamical and microphysical variables in observed Florida convective storms using a cloud model and its adjoint. Preprints, *18th Conf. on Severe Local Storms,* San Francisco, CA, Amer. Meteor. Soc., 555–559.

——, D. W. Flicker, and D. K. Lilly, 1991: Recovery of three-dimensional wind and temperature fields from single-Doppler radar data. *J. Atmos. Sci.,* **48,** 876–890.

——, N. A. Crook, and L. J. Miller, 1995: Retrieval of the dynamical and microphysical structure of convective storms in CAPE using a cloud model and its adjoint. Preprints, *27th Conf. on Radar Meteorology,* Vail, CO, Amer. Meteor. Soc., 820–822.

Talagrand, O., and P. Courtier, 1987: Variational assimilation of meteorological observations with the adjoint vorticity equation—Part I. Theory. *Quart. J. Roy. Meteor. Soc.,* **113,** 1311–1328.

Tripoli, G. J., and W. R. Cotton, 1981: The use of ice-liquid water potential temperature as a thermodynamic variable in deep atmospheric models. *Mon. Wea. Rev.,* **109,** 1094–1102.

Tuttle, J. D., and G. B. Foote, 1990: Determination of the boundary-layer airflow from a single Doppler radar. *J. Atmos. Oceanic. Technol.,* **7,** 218–232.

Verlinde, J., and W. R. Cotton, 1990: A critical look at kinematic microphysical retrieval algorithms. Preprints, *Conf. on Cloud Physics,* San Francisco, CA, Amer. Meteor. Soc., 453–457.

——, and ——, 1993: Fitting microphysical observations of nonsteady convective clouds to a numerical model: An application of the adjoint technique of data assimilation to a kinematic model. *Mon. Wea. Rev.,* **121,** 2776–2793.

Vukicevic, T., and R. M. Errico, 1993: Linearization and adjoint of parameterized moist diabatic processes. *Tellus,* **45A,** 493–510.

Xu, Q., 1996a: Generalized adjoint for physical processes with parameterized discontinuities. Part I: Basic and heuristic examples. *J. Atmos. Sci.,* **53,** 1123–1142.

——, 1996b: Generalized adjoint for physical processes with parameterized discontinuities. Part II: Vector formulations and matching conditions. *J. Atmos. Sci.,* **53,** 1143–1155.

Ziegler, C. L., 1985: Retrieval of thermal and microphysical variables in observed convective storms. Part I: Model development and preliminary testing. *J. Atmos. Sci.,* **42,** 1487–1509.

——, 1988: Retrieval of thermal and microphysical variables in observed convective storms. Part II: Sensitivity of cloud processes to variation of the microphysical parameterization. *J. Atmos. Sci.,* **45,** 1072–1090.

Zou, X., 1995: Tangent linear and adjoint of ''on–off'' processes and their feasibility for use in four-dimensional variational data assimilation. *Tellus,* **49A,** (1), 3–31.

——, I. M. Navon, and J. G. Sela, 1993a: Control of gravitational oscillations in variational data assimilation. *Mon. Wea. Rev.,* **121,** 272–289.

——, ——, and ——, 1993b: Variational data assimilation with moist threshold processes using the NMC spectral model. *Tellus,* **45A,** 370–387.

Zupanski, D., and F. Mesinger, 1995: Four-dimensional variational assimilation of precipitation data. *Mon. Wea. Rev.,* **123,** 1112–1127.

Zupanski, M., 1993: Regional four-dimensional variational data assimilation in a quasi-operational forecasting environment. *Mon. Wea. Rev.,* **121,** 2396–2408.